Electronic Supplementary Information for Dalton Transactions

Supporting Information

Comparison of Electronic Structures and Light-Induced Excited Spin State Trapping between $[Fe(2\text{-picolylamine})_3]^{2+}$ and Its Iron(III) Analogue

Hideo Ando,[†] Yoshihide Nakao,[†] Hirofumi Sato,[†] and Shigeyoshi Sakaki*[†‡]

[†]Department of Molecular Engineering, Graduate School of Engineering, Kyoto University, Nishikyo-ku, Kyoto 615-8510, Japan, and [‡]Fukui Institute for Fundamental Chemistry, Kyoto University, Nishi-hiraki cho, Takano, Sakyo-ku, Kyoto 606-8301, Japan

sakaki@moleng.kyoto-u.ac.jp

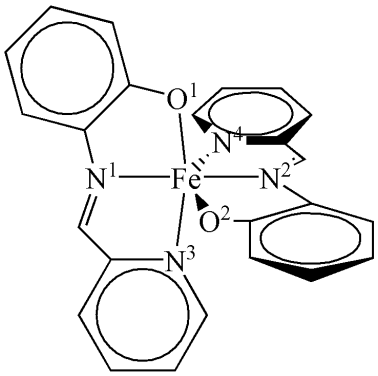

SCHEME S1: Structure of $[Fe^{III}(pap)_2]^+$

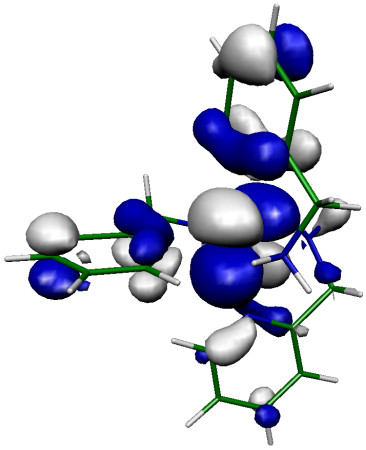

d_{zx} (-12.1 eV)

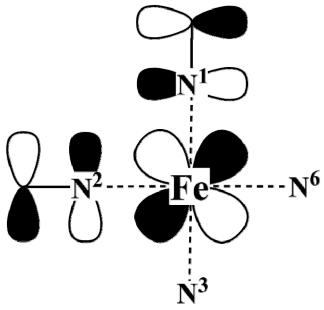

Presence of $d_{\pi} - \pi$ (N^1 and N^2) interaction between Fe and pic

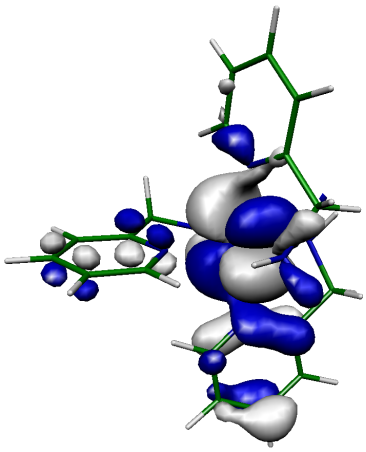

d_{yz} (-12.2 eV)

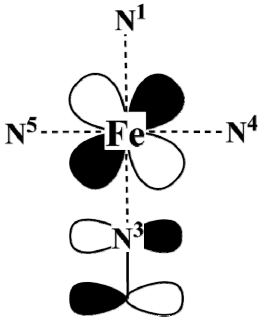

Presence of $d_{\pi} - \pi$ (N^3) interaction between Fe and pic

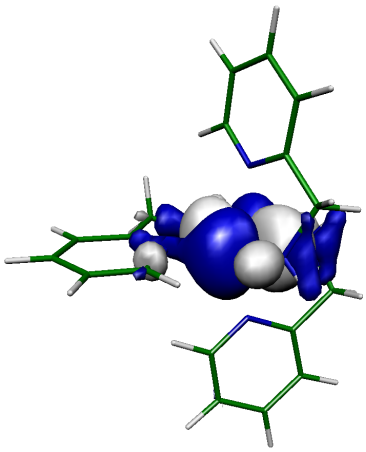

d_{xy} (-12.3 eV)

Absence of $d_{\pi} - \pi$ interaction between Fe and pic

SCHEME S2: Orbital Energy Splitting of t_{2g}-Like d Orbitals of mer-$[Fe^{II}(2\text{-pic})_3]^{2+}$ (Singlet State) by the Anti-Bonding Interaction with the π Orbitals (HOMO-3 Shown in Figure 2) of the Pic Ligands. In Visualizing MOs, the Threshold Value (0.018) of Isosurface Was Set to Be Smaller than That (0.050) Used in Figure 1.

TABLE S1: Relative Energies[a] and Geometrical Parameters of mer-$[Fe^{II}(2\text{-pic})_3]^{2+}$ Optimized with the B3LYP/BS-1 Method

	Singlet (C_1)	Triplet-a (C_1)	Triplet-b (C_1)	Triplet-c (C_1)	Quintet (C_1)	ΔR_{HL}
			Relative Energies /kcal mol^{-1}			
	0.0[a]	8.3	8.8	9.1	-8.9	
			Bond Lengths /Å			
Fe–N^1	2.063 (1.998)[b]	2.189[c]	2.039	2.244	2.247 (2.186)[b]	0.184 (0.188)[b]
Fe–N^2	2.072 (2.014)	2.192	2.230	2.046	2.253 (2.192)	0.181 (0.178)
Fe–N^3	2.055 (1.994)	2.247	2.041	2.168	2.243 (2.182)	0.187 (0.188)
Fe–N^4	2.067 (2.031)	2.051	2.197	2.282	2.268 (2.161)	0.202 (0.130)
Fe–N^5	2.076 (2.019)	2.056	2.297	2.222	2.275 (2.158)	0.199 (0.139)
Fe–N^6	2.073 (2.021)	2.289	2.203	2.059	2.287 (2.170)	0.215 (0.149)
			Bond Angles /deg.			
N^1–Fe–N^2	93.2	102.0	91.1	95.7	101.3	8.1
N^1–Fe–N^3	169.7	161.5	170.7	164.8	160.4	-9.3
N^1–Fe–N^4	80.3 (81.5)	78.7	79.1	74.2	74.1 (76.2)	-6.2 (-5.3)
N^1–Fe–N^5	97.9	99.3	99.9	98.3	99.1	1.2
N^1–Fe–N^6	92.0	90.0	94.7	90.7	90.6	-1.4
N^2–Fe–N^3	95.1	95.2	96.4	95.8	96.2	1.1
N^2–Fe–N^4	96.2	95.9	100.0	96.2	95.6	-0.6
N^2–Fe–N^5	80.7 (81.3)	78.8	74.8	78.8	74.5 (75.9)	-6.2 (-5.4)
N^2–Fe–N^6	171.4	166.0	165.5	171.5	164.9	-6.5
N^3–Fe–N^4	92.8	93.1	94.2	94.8	95.6	2.8
N^3–Fe–N^5	89.4	90.5	87.4	93.6	94.0	4.6
N^3–Fe–N^6	80.5 (81.7)	73.9	79.2	78.9	73.7 (77.0)	-6.7 (-4.7)
N^4–Fe–N^5	176.3	173.8	174.7	170.6	166.9	-9.4
N^4–Fe–N^6	91.4	93.4	94.1	91.0	96.5	5.2
N^5–Fe–N^6	91.9	92.4	91.1	94.7	94.7	2.8

[a] The singlet state at its equilibrium geometry was taken to be standard (energy *zero*).

[b] In parentheses are experimental values.[41b] The singlet and the quintet geometries were determined at 90 K and 150 K, respectively, by X-ray diffraction measurement.

[c] The underlined values correspond to the bond lengths considerably longer than those of the singlet state.

TABLE S2: Relative Energies[a] and Geometrical Parameters of fac-$[Fe^{II}(2\text{-pic})_3]^{2+}$ Optimized with the B3LYP/BS-1 Method

	Singlet (C_1)	Triplet (C_1)	Quintet (C_1)	ΔR_{HL}
	Relative Energies /kcal mol^{-1}			
	0.0[a]	9.4	-7.1	
	Bond Lengths /Å			
Fe–N^1	2.046 (1.979)[b]	2.027	2.227[c]	0.181
Fe–N^2	2.042 (1.987)	2.155	2.225	0.184
Fe–N^3	2.050 (1.991)	2.235	2.243	0.194
Fe–N^4	2.078 (2.030)	2.231	2.282	0.204
Fe–N^5	2.078 (2.021)	2.061	2.287	0.209
Fe–N^6	2.080 (2.026)	2.280	2.277	0.196
	Bond Angles /deg.			
N^1–Fe–N^2	94.9 (94.7)	96.0	97.1	2.1
N^1–Fe–N^3	96.3 (96.2)	97.6	97.0	0.8
N^1–Fe–N^4	81.0 (82.3)	79.4	75.0	-5.9
N^1–Fe–N^5	173.5 (174.0)	173.5	168.3	-5.2
N^1–Fe–N^6	91.1 (90.3)	91.1	95.1	4.0
N^2–Fe–N^3	95.8 (95.4)	99.2	98.8	3.0
N^2–Fe–N^4	90.8 (89.8)	94.7	94.1	3.2
N^2–Fe–N^5	80.6 (83.1)	79.1	74.2	-6.4
N^2–Fe–N^6	173.4 (174.0)	171.4	166.8	-6.6
N^3–Fe–N^4	173.0 (174.7)	166.1	165.7	-7.3
N^3–Fe–N^5	89.0 (89.6)	87.5	92.1	3.1
N^3–Fe–N^6	80.9 (80.8)	75.1	74.8	-6.2
N^4–Fe–N^5	94.2 (92.1)	96.6	97.5	3.3
N^4–Fe–N^6	92.7 (94.2)	91.2	93.8	1.2
N^5–Fe–N^6	93.6 (92.3)	94.2	94.3	0.8

[a] The singlet state at its equilibrium geometry was taken to be standard (energy *zero*).

[b] In parentheses are experimental values.[40a]

[c] The underlined values correspond to the bond lengths considerably longer than those of the singlet state.

TABLE S3: Relative Energies[a] and Geometrical Parameters of mer-$[Fe^{III}(2\text{-pic})_3]^{3+}$ Optimized with the B3LYP/BS-1 Method

	Doublet (C_1)	Quartet-a (C_1)	Quartet-b (C_1)	Quartet-c (C_1)	Sextet (C_1)	ΔR_{HL}
			Relative Energies /kcal mol^{-1}			
	0.0[a]	8.5	8.7	8.9	1.6	
			Bond Lengths /Å			
Fe–N^1	2.015	2.017	2.060	2.231[b]	2.161	0.146
Fe–N^2	2.019	2.224	2.066	2.010	2.155	0.136
Fe–N^3	2.040	2.065	2.028	2.202	2.145	0.105
Fe–N^4	2.039	2.053	2.267	2.094	2.199	0.160
Fe–N^5	2.039	2.088	2.279	2.068	2.204	0.165
Fe–N^6	2.047	2.271	2.056	2.084	2.229	0.182
			Bond Angles /deg.			
N^1–Fe–N^2	95.0	96.3	93.6	98.8	99.5	4.5
N^1–Fe–N^3	166.5	165.7	168.1	162.6	159.8	−6.8
N^1–Fe–N^4	80.8	81.0	76.6	76.5	75.9	−4.8
N^1–Fe–N^5	96.6	97.3	95.6	95.0	95.8	−0.8
N^1–Fe–N^6	90.0	90.7	91.2	88.4	88.6	−1.4
N^2–Fe–N^3	96.1	97.1	95.8	96.8	98.3	2.3
N^2–Fe–N^4	93.7	94.4	95.0	95.1	94.6	0.9
N^2–Fe–N^5	81.1	76.7	76.5	80.5	76.0	−5.2
N^2–Fe–N^6	171.7	168.8	170.2	171.2	166.6	−5.1
N^3–Fe–N^4	90.9	92.8	95.2	94.4	93.2	2.3
N^3–Fe–N^5	92.7	90.9	93.8	95.2	97.7	5.0
N^3–Fe–N^6	79.9	77.0	80.6	76.8	75.8	−4.1
N^4–Fe–N^5	174.0	170.7	168.3	169.8	166.4	−7.6
N^4–Fe–N^6	93.6	95.3	94.4	91.5	97.7	4.2
N^5–Fe–N^6	91.8	93.8	94.5	93.8	92.7	0.9

[a] The doublet state at its equilibrium geometry was taken to be standard (energy *zero*).

[b] The underlined values correspond to the bond lengths considerably longer than those of the doublet state.

TABLE S4: Relative Energies[a] and Geometrical Parameters of fac-$[Fe^{III}(2\text{-pic})_3]^{3+}$ Optimized with the B3LYP/BS-1 Method

	Doublet (C_1)	Quartet (C_1)	Sextet (C_1)	ΔR_{HL}
		Relative Energies /kcal mol^{-1}		
	0.0[a]	9.0	2.1	
		Bond Lengths /Å		
Fe–N^1	2.012	2.052	2.125[b]	0.113
Fe–N^2	2.014	2.002	2.128	0.114
Fe–N^3	2.014	2.196	2.135	0.121
Fe–N^4	2.052	2.290	2.231	0.179
Fe–N^5	2.051	2.078	2.226	0.175
Fe–N^6	2.053	2.088	2.235	0.182
		Bond Angles /deg.		
N^1–Fe–N^2	96.3	95.1	97.7	1.4
N^1–Fe–N^3	97.3	100.6	99.7	2.4
N^1–Fe–N^4	81.7	77.9	76.9	−4.8
N^1–Fe–N^5	174.6	168.8	166.0	−8.6
N^1–Fe–N^6	88.9	89.9	95.7	6.8
N^2–Fe–N^3	97.3	98.1	99.5	2.2
N^2–Fe–N^4	88.5	94.3	94.4	5.9
N^2–Fe–N^5	81.0	81.2	76.6	−4.4
N^2–Fe–N^6	174.8	174.1	166.5	−8.3
N^3–Fe–N^4	174.2	167.5	166.1	−8.2
N^3–Fe–N^5	87.7	90.4	93.9	6.2
N^3–Fe–N^6	81.6	77.8	76.6	−5.0
N^4–Fe–N^5	93.5	91.8	90.6	−2.9
N^4–Fe–N^6	92.7	89.7	90.2	−2.5
N^5–Fe–N^6	93.8	94.5	90.7	−3.2

[a] The doublet state at its equilibrium geometry was taken to be standard (energy *zero*).

[b] The underlined values correspond to the bond lengths considerably longer than those of the doublet state.

TABLE S5: Several Stable Conformations with NH_2 Libration. Relative Energies[a] and Geometrical Parameters of mer-$[Fe^{II}(2\text{-pic})_3]^{2+}$ Optimized with the B3LYP/BS-1 Method

	Singlet Geometries							
	(R,R,R)[b]	(R,R,L)	(R,L,R)	(L,R,R)	(R,L,L)	(L,R,L)	(L,L,R)	(L,L,L)
	Relative Energies /kcal mol^{-1}							
	−0.6	−1.5	0.0[a]	0.4	0.1	0.0	−1.8	−1.3
	Bond Lengths /Å							
Fe–N^1	2.059	2.060	2.063	2.065	2.058	2.068	2.058	2.056
Fe–N^2	2.064	2.059	2.072	2.060	2.073	2.052	2.062	2.066
Fe–N^3	2.048	2.042	2.055	2.049	2.052	2.039	2.056	2.057
Fe–N^4	2.061	2.062	2.067	2.065	2.067	2.069	2.072	2.071
Fe–N^5	2.076	2.076	2.076	2.078	2.077	2.076	2.075	2.076
Fe–N^6	2.073	2.077	2.073	2.073	2.076	2.078	2.072	2.072
	Quintet Geometries							
	(R,R,R)[b]	(R,R,L)	(R,L,R)	(L,R,R)	(R,L,L)	(L,R,L)	(L,L,R)	(L,L,L)
	Relative Energies /kcal mol^{-1}							
	0.2	−0.2	0.0[a]	0.2	0.2	−0.1	−1.0	−0.6
	Bond Lengths /Å							
Fe–N^1	2.233	2.230	2.247	2.246	2.247	2.231	2.237	2.235
Fe–N^2	2.244	2.241	2.253	2.259	2.251	2.253	2.246	2.248
Fe–N^3	2.231	2.230	2.243	2.233	2.240	2.228	2.232	2.227
Fe–N^4	2.275	2.277	2.268	2.282	2.271	2.287	2.283	2.286
Fe–N^5	2.281	2.277	2.275	2.275	2.275	2.269	2.275	2.274
Fe–N^6	2.290	2.297	2.287	2.290	2.292	2.303	2.285	2.295

[a] The equilibrium geometries shown in Tables 1 and S1 were taken to be standard. These geometries were employed in evaluation of PESs. [b] See the following pictures for the abbreviations which represent conformations. In the (R,L,R) conformation, for example, the pic ligand including N^1 and N^4 atoms (see Scheme 3A for N^α atoms), that including N^2 and N^5 atoms, and that including N^3 and N^6 atoms have an R-type, L-type, and R-type conformation, respectively.

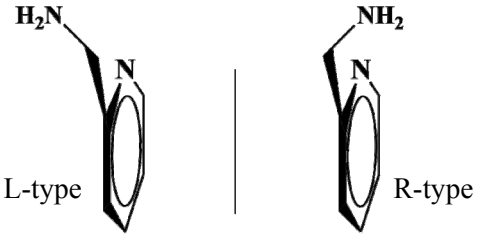

TABLE S6: Relative Energies[a] and Geometrical Parameters of mer-$[Fe^{II}(2\text{-pic})_3]^{2+}$ Optimized with the B3LYP*/BS-1 and the PBE0/BS-1 Methods

	B3LYP*			PBE0		
	Singlet (C_1)	Quintet (C_1)	ΔR_{HL}	Singlet (C_1)	Quintet (C_1)	ΔR_{HL}
			Relative Energies /kcal mol^{-1}			
	0.0[a]	−3.7		0.0[a]	−18.6	
			Bond Lengths /Å			
Fe–N^1	2.048	2.242	0.194	2.041	2.226	0.185
Fe–N^2	2.055	2.246	0.191	2.064	2.225	0.161
Fe–N^3	2.040	2.237	0.197	2.034	2.225	0.191
Fe–N^4	2.057	2.263	0.206	2.057	2.251	0.194
Fe–N^5	2.066	2.270	0.204	2.070	2.255	0.185
Fe–N^6	2.064	2.282	0.218	2.069	2.268	0.199
			Bond Angles /deg.			
N^1–Fe–N^2	93.2	101.3	8.2	93.1	102.5	9.4
N^1–Fe–N^3	169.9	160.4	−9.5	169.8	160.4	−9.4
N^1–Fe–N^4	80.5	74.2	−6.3	80.2	74.1	−6.1
N^1–Fe–N^5	97.7	98.8	1.1	98.1	98.7	0.6
N^1–Fe–N^6	91.8	90.4	−1.4	92.1	90.3	−1.8
N^2–Fe–N^3	95.0	96.3	1.2	95.1	95.0	0.0
N^2–Fe–N^4	96.1	95.4	−0.7	96.3	95.7	−0.6
N^2–Fe–N^5	81.1	74.6	−6.4	80.6	74.8	−5.8
N^2–Fe–N^6	171.7	165.2	−6.5	171.4	164.5	−6.8
N^3–Fe–N^4	92.7	95.6	2.9	92.8	95.6	2.8
N^3–Fe–N^5	89.4	94.2	4.8	89.2	94.3	5.1
N^3–Fe–N^6	80.7	73.8	−6.9	80.5	73.9	−6.6
N^4–Fe–N^5	176.6	166.7	−9.9	176.4	166.8	−9.6
N^4–Fe–N^6	91.2	96.5	5.3	91.3	96.0	4.7
N^5–Fe–N^6	91.7	94.8	3.1	91.9	95.0	3.1

[a] The singlet state at its equilibrium geometry was taken to be standard (energy *zero*).

TABLE S7: Relative Energies[a] and Geometrical Parameters of $[Fe^{III}(pap)_2]^+$ Optimized with the B3LYP/BS-3[b] Method

	Doublet (C_2)	Quartet (C_1)	Sextet (C_1)	ΔR_{HL}
		Relative Energies /kcal mol^{-1}		
	0.0[a]	14.0	4.2	
		Bond Lengths /Å		
Fe–O^1	1.869 (1.882)[c]	1.868	1.921 (1.931)[c]	0.053 (0.049)[c]
Fe–O^2	1.869 (1.883)	1.949[d]	1.921 (1.932)	0.053 (0.049)
Fe–N^1	1.934 (1.915)	1.963	2.195 (2.136)	0.261 (0.221)
Fe–N^2	1.934 (1.911)	2.084	2.195 (2.105)	0.261 (0.194)
Fe–N^3	2.019 (1.993)	2.049	2.252 (2.138)	0.233 (0.145)
Fe–N^4	2.019 (1.994)	2.311	2.252 (2.202)	0.233 (0.208)
		Bond Angles /deg.		
O^1–Fe–O^2	95.3 (93.6)	98.6	100.7 (96.7)	5.4 (3.1)
O^1–Fe–N^1	85.4 (85.7)	84.6	77.2 (80.0)	−8.2 (−5.7)
O^1–Fe–N^2	90.9 (91.6)	92.2	110.5 (109.4)	19.6 (17.8)
O^1–Fe–N^3	166.5 (166.4)	164.3	150.1 (154.5)	−16.4 (−11.9)
O^1–Fe–N^4	88.8 (90.0)	87.5	91.8 (92.6)	3.0 (2.6)
O^2–Fe–N^1	90.9 (92.0)	104.6	110.5 (113.6)	19.6 (21.6)
O^2–Fe–N^2	85.4 (85.7)	80.1	77.2 (78.7)	−8.2 (−7.0)
O^2–Fe–N^3	88.8 (90.5)	91.4	91.8 (91.2)	3.0 (0.7)
O^2–Fe–N^4	166.5 (166.3)	154.2	150.1 (153.4)	−16.4 (−12.9)
N^1–Fe–N^2	174.5 (176.4)	174.7	168.4 (164.1)	−6.1 (−12.3)
N^1–Fe–N^3	81.6 (81.2)	81.2	73.0 (74.6)	−8.6 (−6.6)
N^1–Fe–N^4	102.3 (101.4)	101.0	98.6 (92.6)	−3.7 (−8.8)
N^2–Fe–N^3	102.3 (101.7)	101.4	98.6 (95.9)	−3.7 (−5.8)
N^2–Fe–N^4	81.6 (81.0)	74.6	73.0 (74.6)	−8.6 (−6.4)
N^3–Fe–N^4	90.2 (89.0)	88.7	90.5 (91.1)	0.4 (2.1)

[a] The doublet state at its equilibrium geometry was taken to be standard (energy *zero*). [b] The usual LANL2DZ basis set with ECPs and the cc-pVDZ basis sets were used for Fe and the other atoms, respectively. [c] In parentheses are experimental values (Juhász, G. *et al.*, *Chem. Phys. Lett.*, 2002, **364**, 164.). [d] The underlined values correspond to the bond lengths considerably longer than those of the doublet state.

TABLE S8: Relative Energies[a] and Geometrical Parameters of [$Fe^{II}(pap)_2$] Optimized with the B3LYP/BS-3[b] Method

	Singlet (C_2)	Triplet (C_1)	Quintet (C_1)	Quintet (C_2)[c]	ΔR_{HL}
		Relative Energies /kcal mol^{-1}			
	0.0[a]	7.9	−3.0	−2.6	
		Bond Lengths /Å			
Fe−O^1	1.987	2.046[d]	2.005[d]	2.055	0.018
Fe−O^2	1.987	2.044	2.111	2.055	0.123
Fe−N^1	1.923	1.948	2.204	2.211	0.281
Fe−N^2	1.923	1.948	2.201	2.211	0.278
Fe−N^3	2.021	2.223	2.313	2.307	0.293
Fe−N^4	2.021	2.221	2.305	2.307	0.284
		Bond Angles /deg.			
O^1−Fe−O^2	91.4	101.9	104.2	102.2	12.8
O^1−Fe−N^1	83.5	82.5	77.1	76.6	−6.4
O^1−Fe−N^2	93.7	95.3	113.6	114.1	19.9
O^1−Fe−N^3	165.2	159.3	149.3	149.2	−16.0
O^1−Fe−N^4	89.3	87.7	94.8	92.8	5.4
O^2−Fe−N^1	93.7	95.3	105.3	114.1	11.6
O^2−Fe−N^2	83.5	82.5	76.5	76.6	−7.1
O^2−Fe−N^3	89.3	87.7	87.2	92.8	−2.1
O^2−Fe−N^4	165.2	159.4	149.0	149.2	−16.2
N^1−Fe−N^2	176.1	176.5	168.6	163.9	−7.4
N^1−Fe−N^3	81.7	78.4	72.3	72.7	−9.4
N^1−Fe−N^4	101.0	104.1	102.6	95.4	1.6
N^2−Fe−N^3	101.0	104.1	96.7	95.4	−4.3
N^2−Fe−N^4	81.7	78.4	73.5	72.7	−8.1
N^3−Fe−N^4	93.7	89.4	88.7	87.5	−5.0

[a] The singlet state at its equilibrium geometry was taken to be standard (energy *zero*). [b] The usual LANL2DZ basis set with ECPs and the cc-pVDZ basis sets were used for Fe and the other atoms, respectively. [c] The C_2-symmetric quintet geometry has an imaginary *b* mode and is not the equilibrium one. [d] The values with normal underlines correspond to the bond lengths considerably longer than those of the singlet state. The values with broken underlines correspond to the bond lengths moderately longer.

TABLE S9: Relative Energies[a] and Geometrical Parameters of $[Fe^{II}(NH_3)_6]^{2+}$ and $[Fe^{III}(NH_3)_6]^{3+}$ Optimized with the B3LYP/BS-1 Method. In Parentheses Are the Relative Energies Evaluated with the CCSD(T)/BS-1 Method.

	$[Fe^{II}(NH_3)_6]^{2+}$			$[Fe^{III}(NH_3)_6]^{3+}$		
	Singlet	Triplet	Quintet	Doublet	Quartet	Sextet
	Relative Energies /kcal mol^{-1}					
	0.0[a]	5.5	-14.0	0.0[a]	5.6	-3.2
	Bond Lengths /Å					
$Fe-N^1$	2.105	2.077	2.282[b]	2.067	2.306	2.221
$Fe-N^2$	2.105	2.269	2.303	2.064	2.082	2.221
$Fe-N^3$	2.105	2.258	2.293	2.064	2.081	2.220
$Fe-N^4$	2.105	2.267	2.282	2.068	2.080	2.221
$Fe-N^5$	2.105	2.284	2.302	2.068	2.080	2.221
$Fe-N^6$	2.105	2.078	2.286	2.067	2.306	2.221

[a] The LS states at their equilibrium geometries were taken to be standard (energy *zero*).

[b] The underlined values correspond to the bond lengths considerably longer than those of the LS states.

Definition of the N^{α} notation

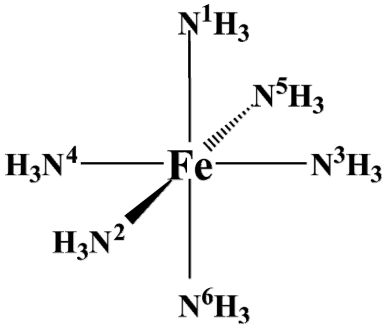

TABLE S10: Excitation Energies (eV) and Oscillator Strengths[a] of fac-[Fe^{II}(2-pic)$_3$]$^{2+}$ in the Singlet and Quintet States (the B3LYP/BS-2 Calculation)

Energies (Oscillator Strengths)	Assignments
Singet States	
2.09 (1.0×10^{-4}), 2.10 (0.0×10^{-4}), 2.12 (1.0×10^{-4}), 3.13 (6.0×10^{-4}), 3.15 (2.0×10^{-4}), 3.19 (2.0×10^{-4})	d-d ($t_{2g}\rightarrow e_g$)
3.91 (1.8×10^{-2}), 3.95 (4.1×10^{-2}), 3.95 (3.1×10^{-2}), 3.96 (5.8×10^{-2}), 4.18 (1.3×10^{-2})	MLCT ($t_{2g}\rightarrow\pi^*_{LUMO}$)[b]
Quintet States	
1.49 (0.0×10^{-4}), 1.65 (0.0×10^{-4})	d-d ($t_{2g}\rightarrow e_g$)

[a] We summarized the excitations with energies ranging from 0.3 to 4.6 eV and omitted charge-transfer transitions whose oscillator strengths are smaller than 0.01.

[b] See Figure 2 for the LUMO of the pic ligand.

TABLE S11: Excitation Energies (eV) and Oscillator Strengths[a] of mer-$[Fe^{III}(2\text{-pic})_3]^{3+}$ in the Doublet and Sextet States (the B3LYP/BS-2 Calculation)

Energies (Oscillator Strengths)	Assignments
Doublet States	
1.38 (0.0×10^{-4}), 1.55 (0.0×10^{-4}), 1.77 (1.0×10^{-4}), 1.90 (0.0×10^{-4}), 2.45 (1.0×10^{-4}), 2.62 (2.0×10^{-4})	d-d ($t_{2g}\rightarrow e_g$)
3.47 (3.2×10^{-2}), 3.69 (1.2×10^{-2})	LMCT ($\pi_{HOMO-3}\rightarrow t_{2g}$, $\pi_{HOMO-2}\rightarrow e_g$)[b]
Sextet States	
2.64 (1.4×10^{-2}), 2.65 (1.1×10^{-2}), 2.66 (1.1×10^{-2}), 2.67 (3.1×10^{-2}), 2.81 (1.5×10^{-2})	LMCT ($\pi_{HOMO-3}\rightarrow t_{2g}$)[b]

[a] We summarized the excitations with energies ranging from 0.6 to 4.3 eV and omitted charge-transfer transitions whose oscillator strengths are smaller than 0.01.

[b] See Figure 2 for the HOMO-3 and HOMO-2 of the pic ligand.

TABLE S12: Excitation Energies (eV) and Oscillator Strengths[a] of fac-[Fe^{III}(2-pic)$_3$]$^{3+}$ in the Doublet and Sextet States (the B3LYP/BS-2 Calculation)

Energies (Oscillator Strengths)	Assignments
Doublet States	
1.48 (0.0×10^{-4}), 1.70 (2.0×10^{-4}), 1.72 (2.0×10^{-4}), 1.96 (0.0×10^{-4}), 2.50 (2.0×10^{-4}), 2.76 (4.0×10^{-4})	d-d ($t_{2g}\rightarrow e_g$)
3.62 (1.0×10^{-2})	LMCT ($\pi_{HOMO-3}\rightarrow t_{2g}$, $\pi_{HOMO-2}\rightarrow e_g$)[b]
Sextet States	
2.70 (2.0×10^{-2}), 2.70 (3.0×10^{-2}), 2.75 (1.4×10^{-2}), 2.83 (1.1×10^{-2})	LMCT ($\pi_{HOMO-3}\rightarrow t_{2g}$)[b]

[a] We summarized the excitations with energies ranging from 0.5 to 4.3 eV and omitted charge-transfer transitions whose oscillator strengths are smaller than 0.01.

[b] See Figure 2 for the HOMO-3 and HOMO-2 of the pic ligand.

Discrepancy in ^{1}MLCT excitation energy between TD-DFT and experimental values

There is large discrepancy in the excitation energy of the ^{1}MLCT transition between the TD-DFT-calculated energy (ca. 4.0 eV) and the experimental value of $[Fe(2\text{-pic})_3]Cl_2$ in ethanol solution (ca. 2.7 eV).[52] As well known, the CT excitation energy can not be calculated correctly with the TD-DFT method when usual functionals are employed. However, this weak point of the TD-DFT calculation is not responsible to the present discrepancy because the TD-DFT calculation with usual functional tends to underestimate the CT excitation energy but the present TD-DFT calculation overestimates the MLCT excitation energy. Thus, we need to consider another factor for this discrepancy. We examined the effects of counter anions (chloride anions) and solvents (ethanol) here. When two Cl^- anions are placed at the same positions as those of the experimental solid structure,[15] the d-d excitation energies are little influenced but the MLCT excitation energies become very close to the experimental values (Table S13A). The solvation effect was evaluated with the PCM method but the CT excitation energies are little influenced by the solvation effect (Table S13B).

TABLE S13: Effects of (A) Two Cl^- Anions and (B) Ethanol in Excitation Energies (eV) and Oscillator Strengths[a] of mer-$[Fe^{II}(2\text{-pic})_3]^{2+}$ in the Singlet State (the B3LYP/BS-1 Calculation)[b]

Energies (Oscillator Strengths)		Assignments
(A) *without* Cl^-	*with* Cl^- [c]	
2.05 (0.0×10^{-4}), 2.08 (0.0×10^{-4}), 2.10 (1.0×10^{-4}), 3.12 (2.0×10^{-4}), 3.15 (1.0×10^{-4}), 3.19 (2.0×10^{-4})	2.36 (2.0×10^{-4}), 2.43 (8.0×10^{-4}), 2.47 (7.0×10^{-4}), 3.72 (4.4×10^{-3})	d-d ($t_{2g}\rightarrow e_g$)
4.01 (7.9×10^{-2}), 4.09 (7.4×10^{-2}), 4.13 (1.2×10^{-2})	2.72 (1.0×10^{-2}), 2.95 (8.6×10^{-2}), 3.27 (1.9×10^{-2})	MLCT ($t_{2g}\rightarrow\pi^*_{LUMO}$)[d]
	3.37 (2.3×10^{-2}), 3.39 (4.1×10^{-2}), 3.49 (4.6×10^{-2})	MLCT ($t_{2g}\rightarrow\pi^*_{LUMO/LUMO+1}$)[d]
(B) *without* ethanol	*with* ethanol[e]	
2.05 (0.0×10^{-4}), 2.08 (0.0×10^{-4}), 2.10 (1.0×10^{-4}), 3.12 (2.0×10^{-4}), 3.15 (1.0×10^{-4}), 3.19 (2.0×10^{-4})	2.06 (0.0×10^{-4}), 2.09 (0.0×10^{-4}), 2.11 (1.0×10^{-4}), 3.09 (6.0×10^{-4}), 3.12 (2.0×10^{-4}), 3.21 (0.0×10^{-4})	d-d ($t_{2g}\rightarrow e_g$)
4.01 (7.9×10^{-2}), 4.09 (7.4×10^{-2}), 4.13 (1.2×10^{-2})	3.73 (8.6×10^{-2}), 3.74 (2.1×10^{-2}), 3.79 (4.4×10^{-2}), 3.80 (4.4×10^{-2}), 3.83 (3.5×10^{-2})	MLCT ($t_{2g}\rightarrow\pi^*_{LUMO}$)[d]

[a] We presented the excitations with energies ranging up to 4.3 eV but omitted charge-transfer (CT) transitions whose oscillator strengths are smaller than 0.01.
[b] We used here the BS-1 set smaller than the BS-2 set but the basis set dependency is small (see Table 3).
[c] The structure is the same as the experimental structure represented by Fepic10K.[15] In the range from 3.3 to 4.3 eV, we also omitted here the CT transitions whose oscillator strengths are smaller than 0.02.
[d] See Figure 2 for the LUMO and the LUMO+1 of the pic ligand.
[e] The PCM method (dielectric constant, $\varepsilon = 24.55$) implemented in Gaussian 03 was employed.

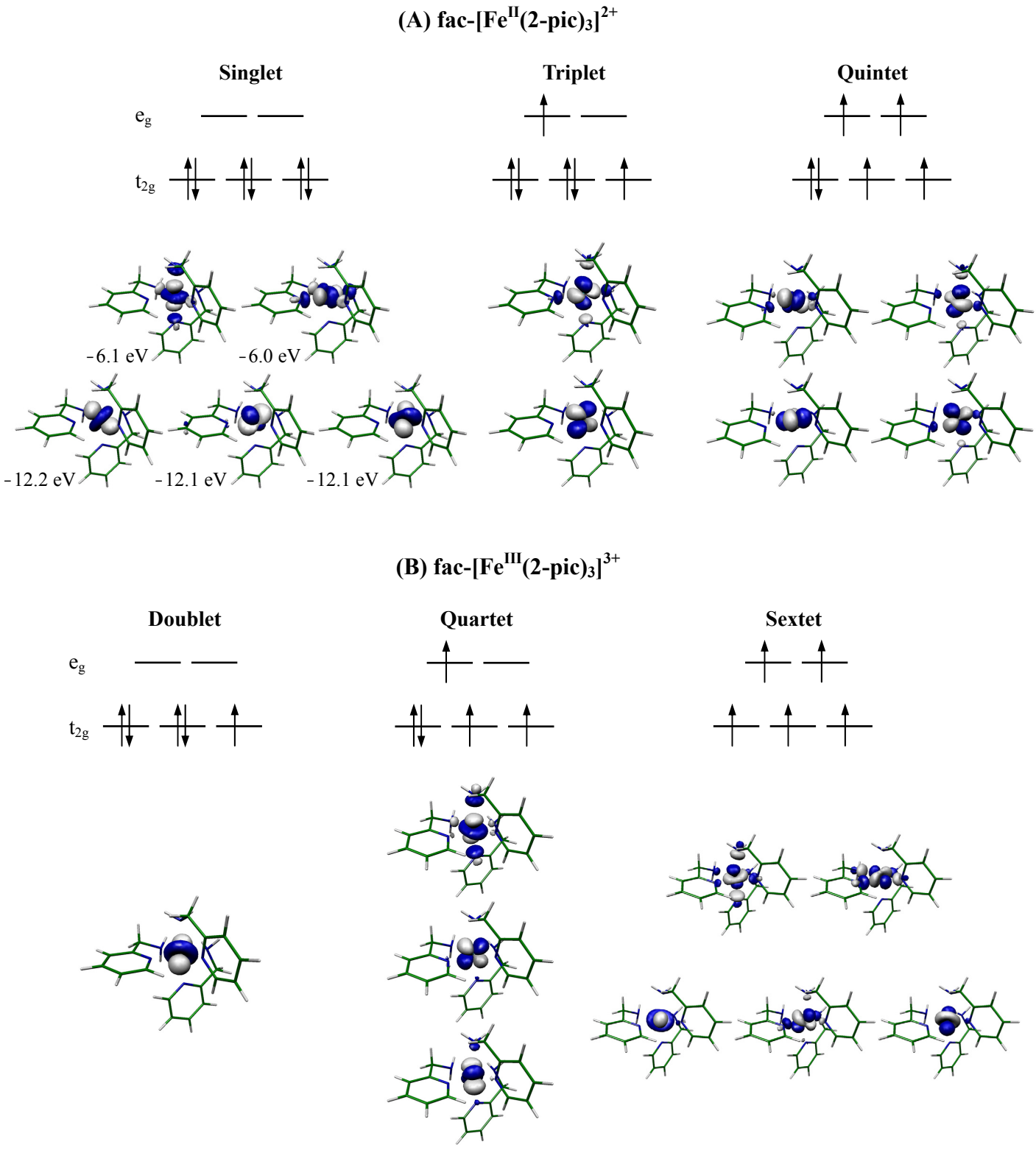

Figure S1. Electron configurations of (A) fac-$[Fe^{II}(2\text{-pic})_3]^{2+}$ and (B) its Fe(III) complex, investigated with the B3LYP/BS-1 method. Five molecular orbitals with Kohn-Sham orbital energies are shown for the singlet state, while only singly-occupied natural orbitals are depicted for the other spin states.

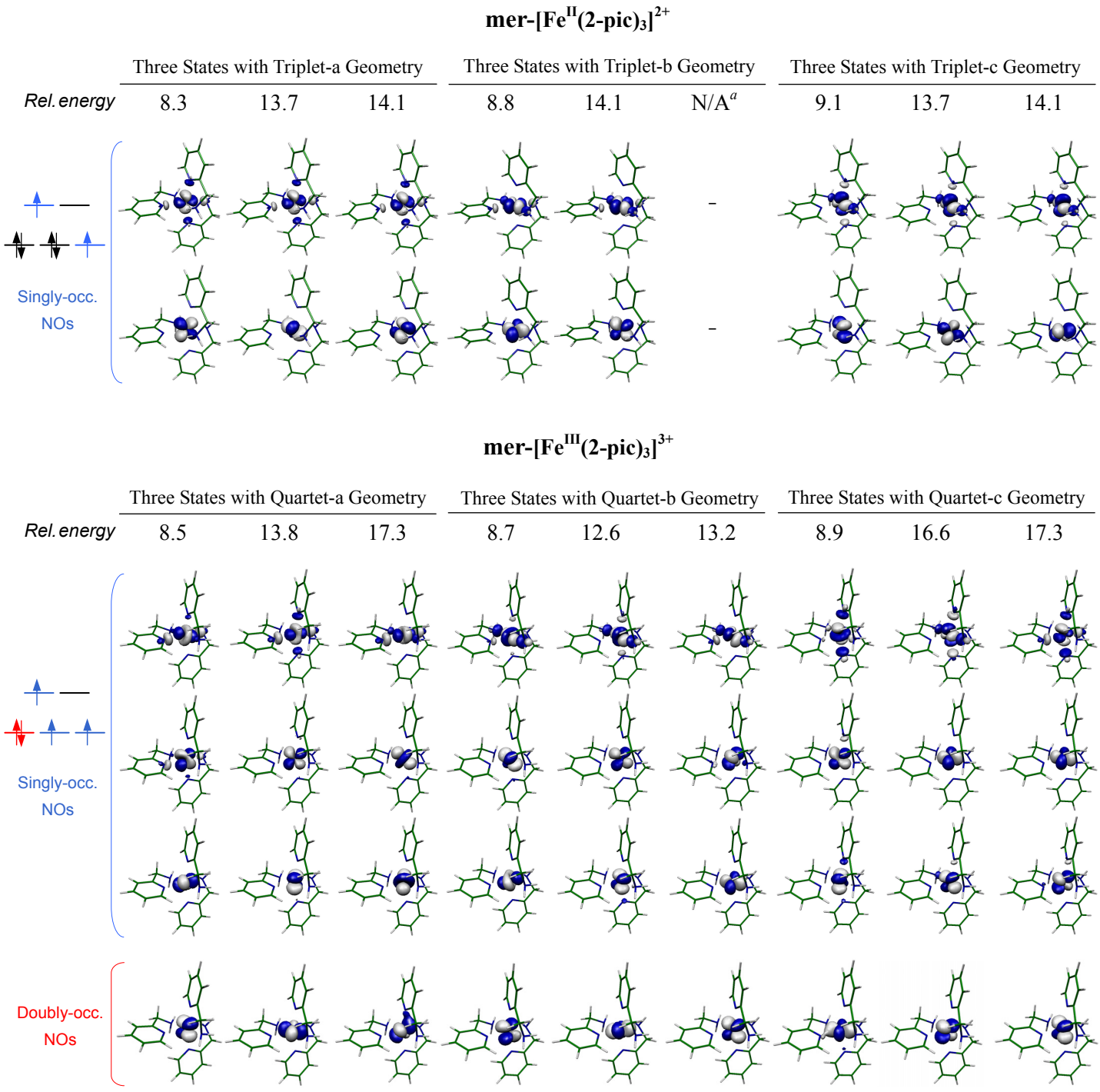

Figure S2A. Relative energies (kcal/mol)[b] of three nearly-degenerate triplet states of mer-$[Fe^{II}(2\text{-pic})_3]^{2+}$ and three nearly-degenerate quartet states of mer-$[Fe^{III}(2\text{-pic})_3]^{3+}$ at each equilibrium geometry, where the B3LYP/BS-1 method was employed. The electron configurations of these states are represented by important d-derived natural orbitals (NOs) whose occupation numbers are very close to 1.0 for the triplet states and either 1.0 or 2.0 for the quartet states.[c]

[a] The SCF did not converge to the standard criterion (10^{-6} hartree), even though we employed the level shift procedure. [b] The LS state at the equilibrium geometry was taken to be standard (energy *zero*). [c] The α-spin canonical MOs are very delocalized; in other words, we could not find clearly d-derived α-spin MOs. On the other hand, NOs are localized. In the triplet states, two d-localized NOs have occupation number of about 1.0. In the quartet states, three d-localized NOs have occupation number of about 1.0 and one d-localized NO has that close to 2.0. Because the β-spin canonical MOs are similar to the corresponding NOs, it is not unreasonable to use NOs to represent the electron configurations of these states.

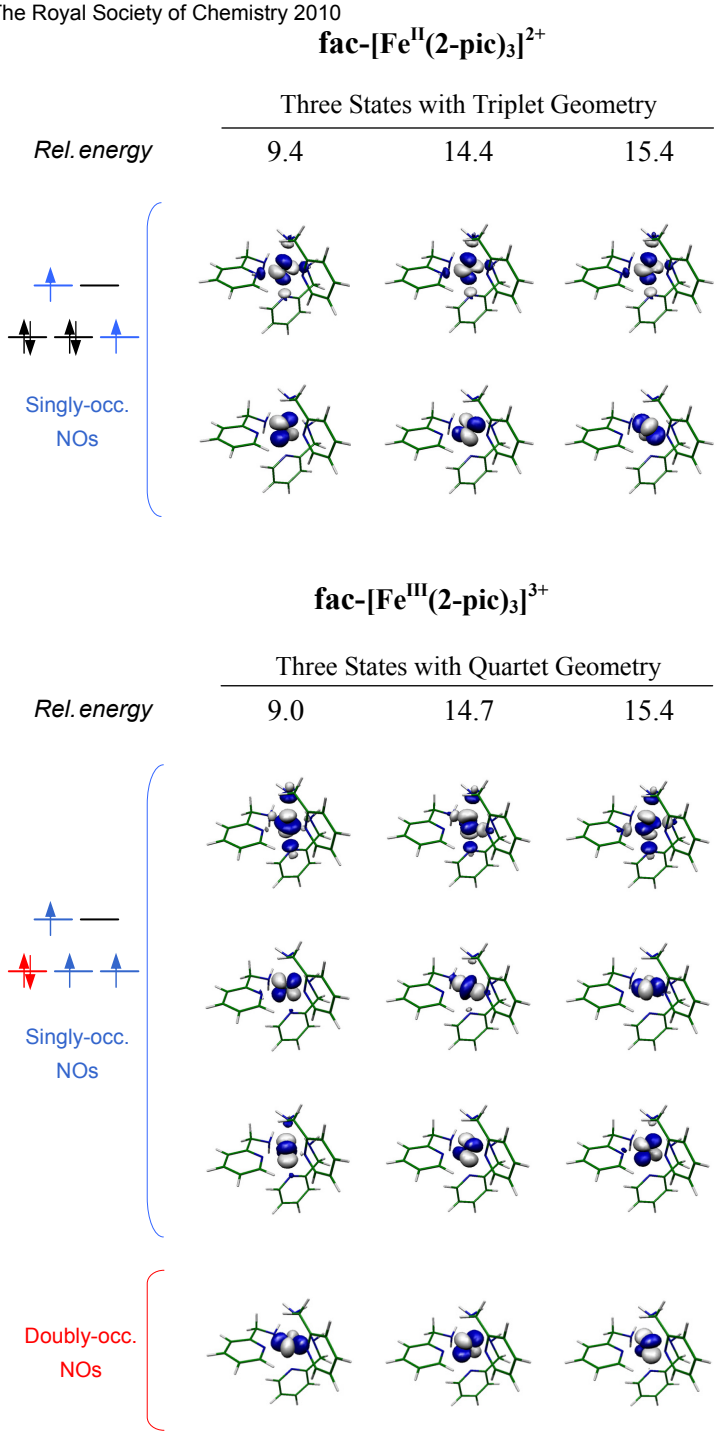

Figure S2B. Relative energies (kcal/mol)[a] of three nearly-degenerate triplet states of fac-$[Fe^{II}(2\text{-pic})_3]^{2+}$ and three nearly-degenerate quartet states of fac-$[Fe^{III}(2\text{-pic})_3]^{3+}$ at each equilibrium geometry, where the B3LYP/BS-1 method was employed. The electron configurations of these states are represented by important d-derived natural orbitals (NOs) whose occupation numbers are very close to 1.0 for the triplet states and either 1.0 or 2.0 for the quartet states.[b]

[a] The LS state at the equilibrium geometry was taken to be standard (energy *zero*). [b] The α-spin canonical MOs are very delocalized; in other words, we could not find clearly d-derived α-spin MOs. On the other hand, NOs are localized. In the triplet states, two d-localized NOs have occupation number of about 1.0. In the quartet states, three d-localized NOs have occupation number of about 1.0 and one d-localized NO has that close to 2.0. Because the β-spin canonical MOs are similar to the corresponding NOs, it is not unreasonable to use NOs to represent the electron configurations of these states.

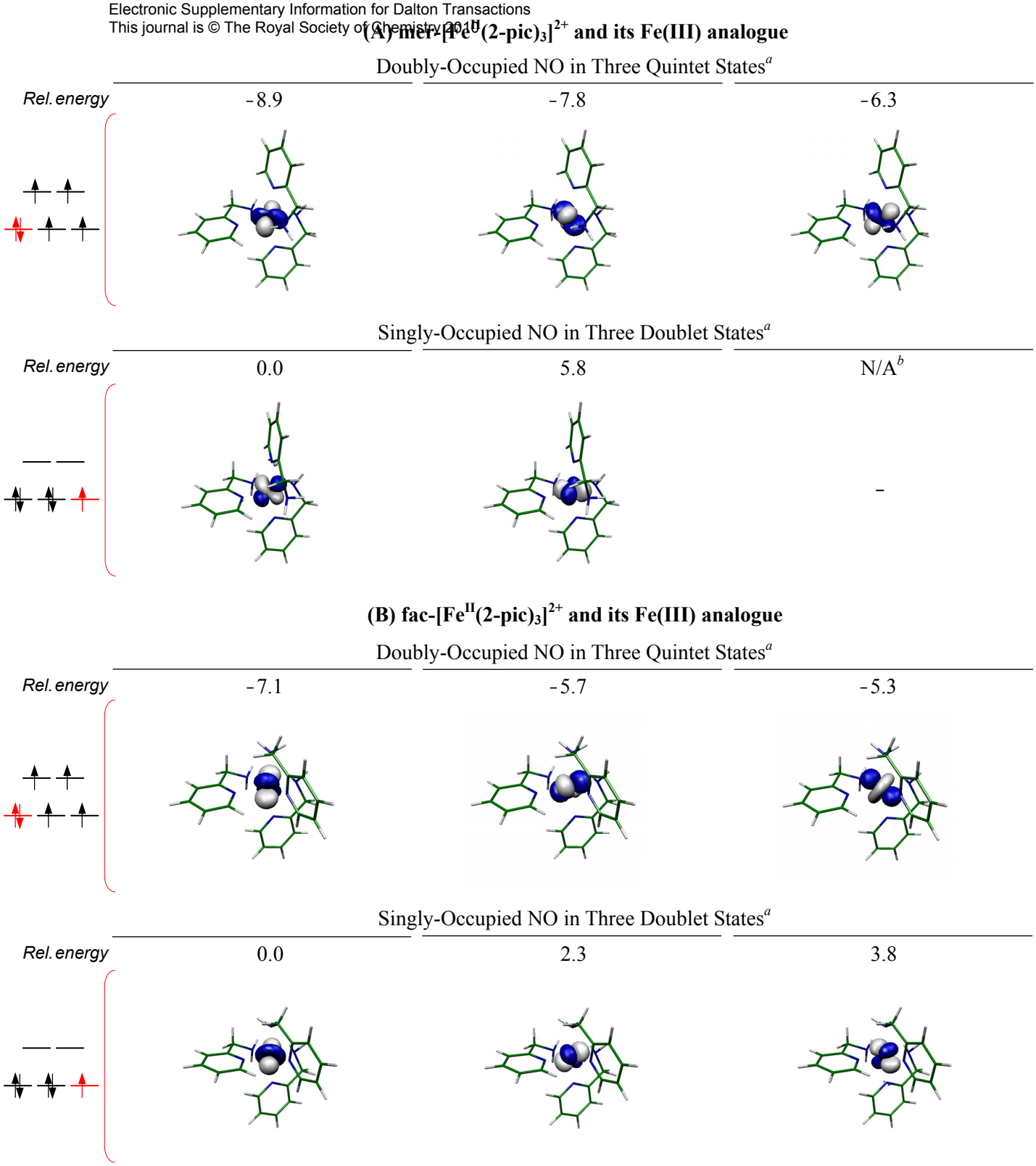

Figure S3. Relative energies (kcal/mol)[c] of three nearly-degenerate doublet states of $[Fe^{III}(2\text{-pic})_3]^{3+}$ and three nearly-degenerate quintet states of $[Fe^{II}(2\text{-pic})_3]^{2+}$ at each equilibrium geometry, where the B3LYP/BS-1 method was employed. The electron configurations of these states are represented by important d-derived natural orbitals (NOs) whose occupation numbers are very close to 2.0 for the quintet states[d] and 1.0 for the doublet states.

[a] Three quintet states and three doublet states were evaluated at the quintet equilibrium geometry (Tables S1 and S2) and the doublet one (Tables S3 and S4), respectively. [b] The SCF did not converge to the standard criterion (10^{-6} hartree), even though we employed the level shift procedure. [c] The LS state at the equilibrium geometry was taken to be standard (energy *zero*). [d] The α-spin canonical MOs are very delocalized; in other words, we could not find clearly d-derived α-spin MOs. On the other hand, NOs are localized. Four d-localized NOs have occupation number of about 1.0 and one d-localized NO has that close to 2.0. Because the β-spin canonical MOs are similar to the corresponding NOs, it is not unreasonable to use NOs to represent the electron configuration of these states.

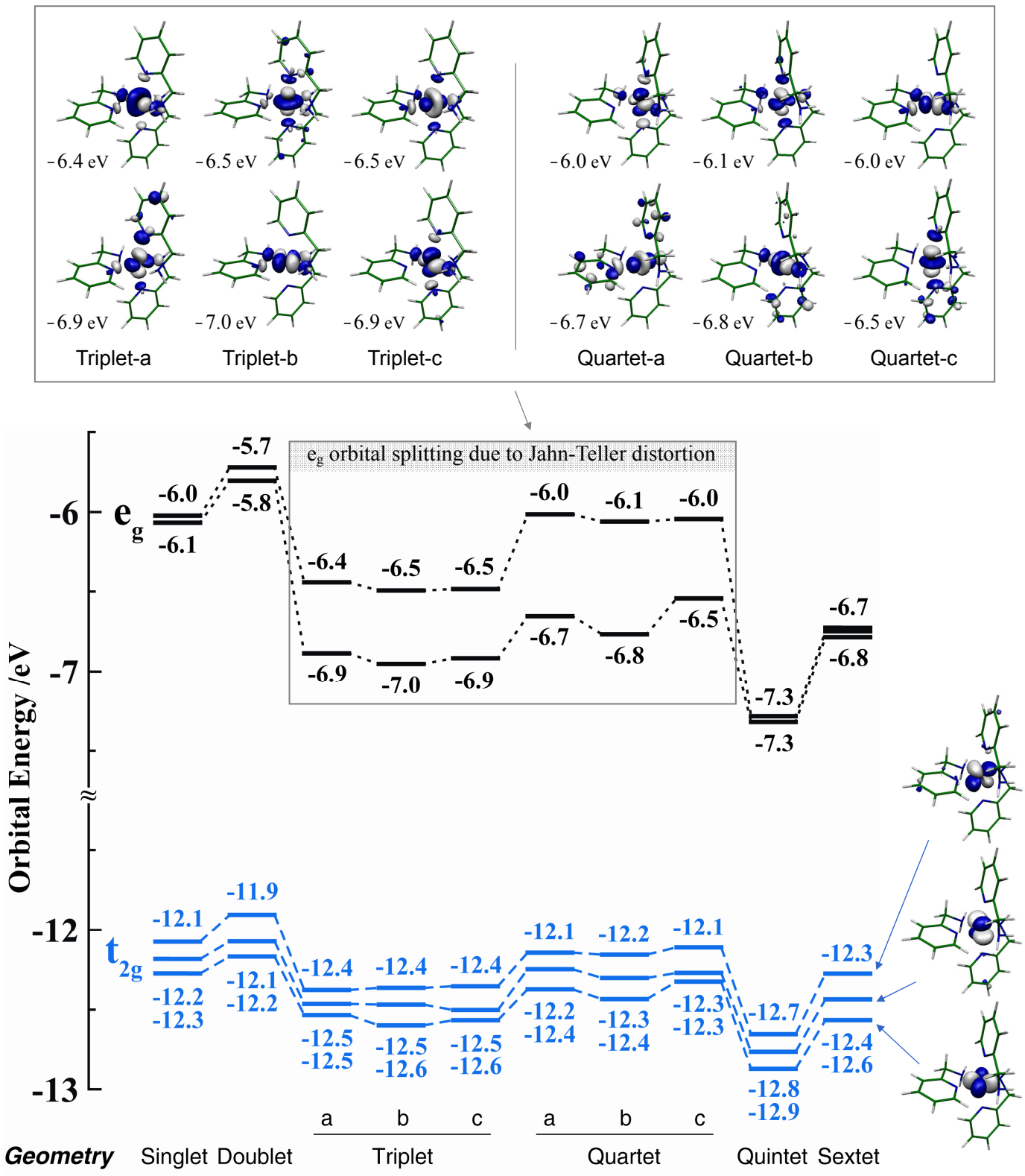

Figure S4. The d orbital energies in the singlet state of mer-$[Fe^{II}(2\text{-pic})_3]^{2+}$ ware summarized for all equilibrium geometries (the B3LYP/BS-1 calculation). The π* orbital energies of the pic ligand are omitted. The character of the e_g-like orbitals changes significantly as geometry changes (see MOs), due to nearly-degeneracy. We, however, *formally* connected their energies using short dash lines (…) for clarification.

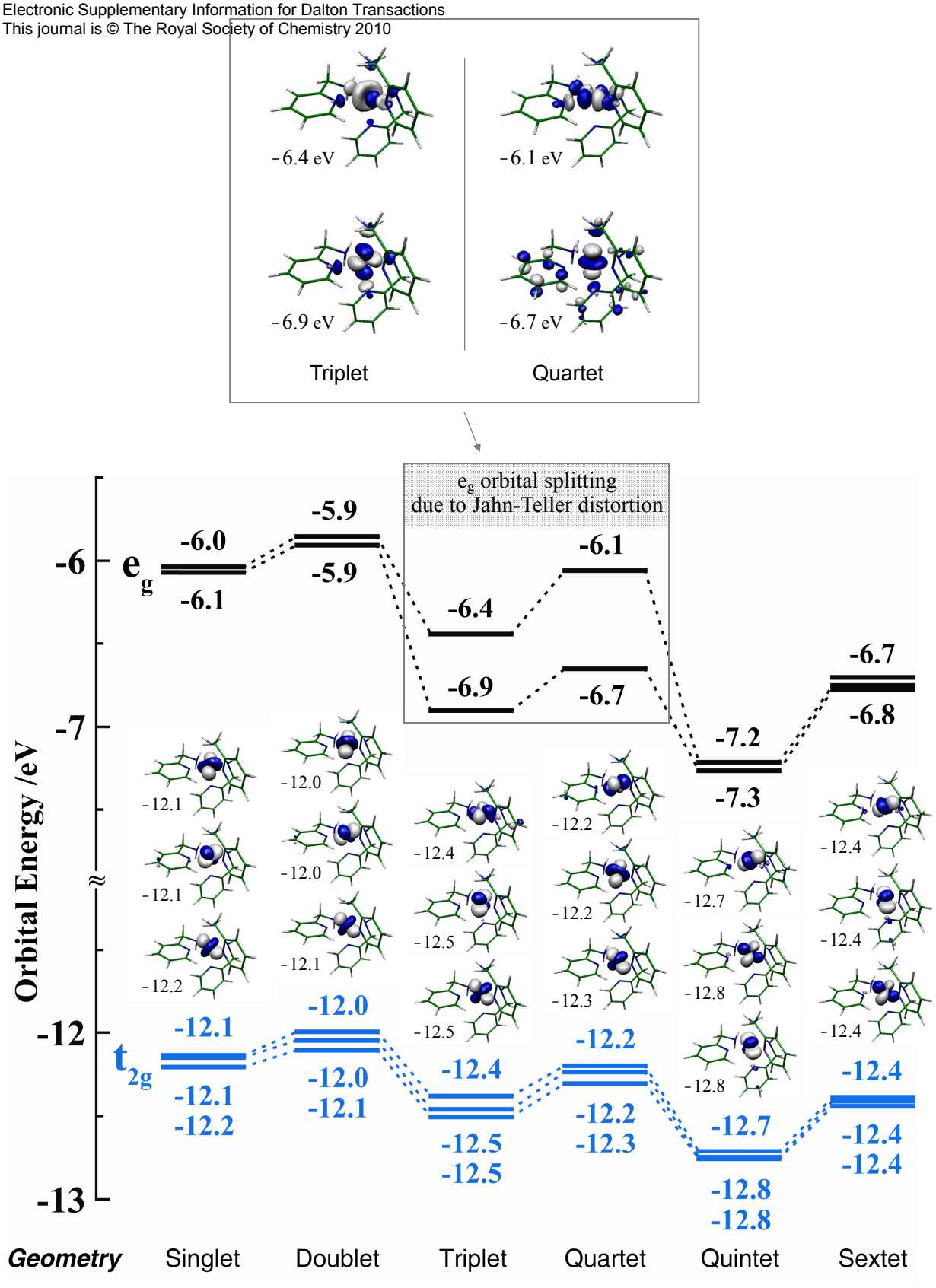

Figure S5. The d orbital energies in the singlet state of fac-$[Fe^{II}(2\text{-pic})_3]^{2+}$ ware summarized for all equilibrium geometries (the B3LYP/BS-1 calculation). The π* orbital energies of the pic ligand are omitted. The character of d orbitals changes significantly as geometry changes (see MOs), due to nearly-degeneracy. We, however, *formally* connected their energies using short dash lines (…) for clarification.

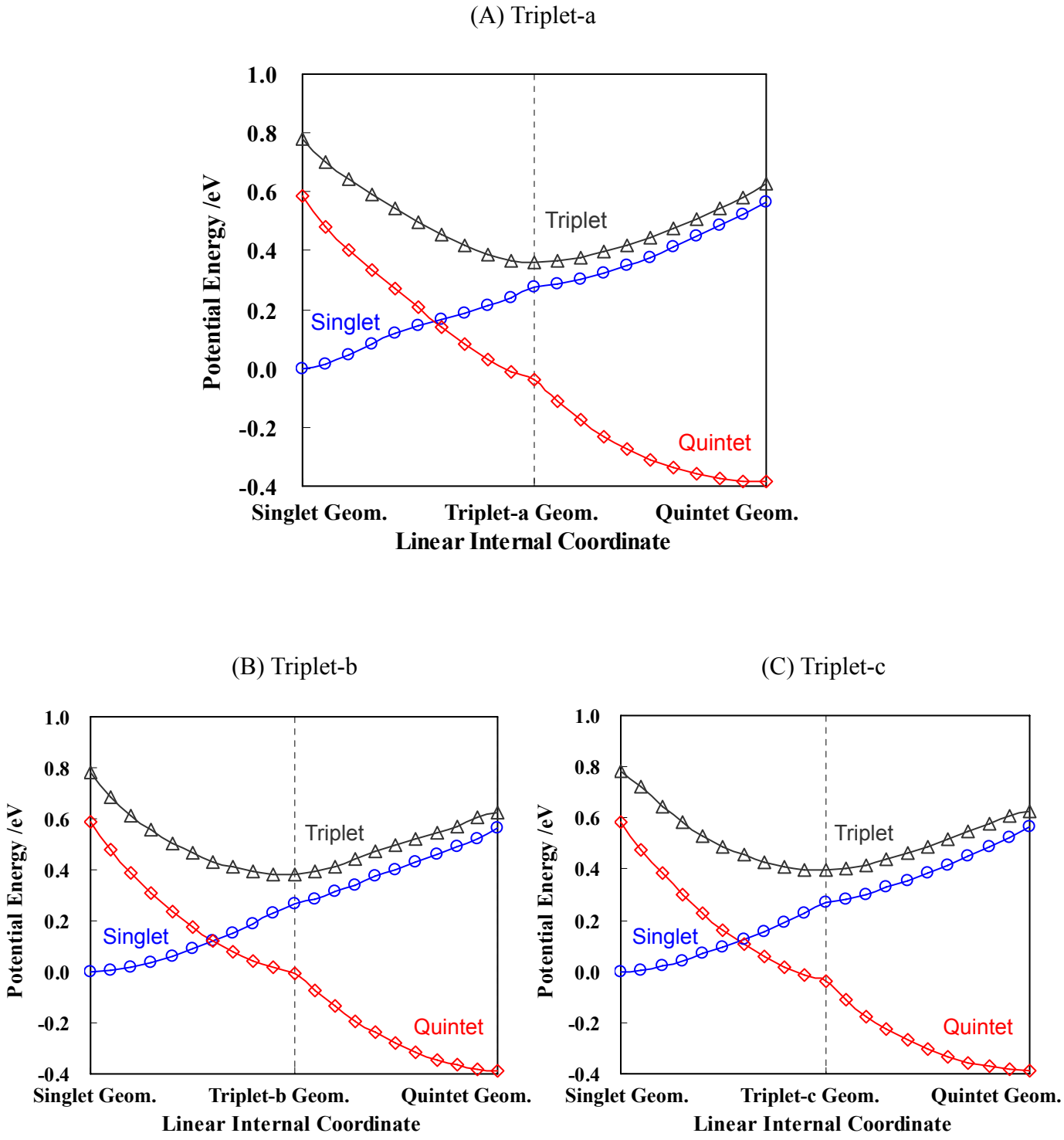

Figure S6. PESs of mer-$[Fe^{II}(2\text{-pic})_3]^{2+}$ in the singlet, triplet, and quintet states (B3LYP/BS-1 calculations). We constructed linear internal coordinates using three Jahn-Teller triplet geometries; (A) the triplet-a, (B) triplet-b, and (C) triplet-c geometries (see Table 1 for these abbreviations).

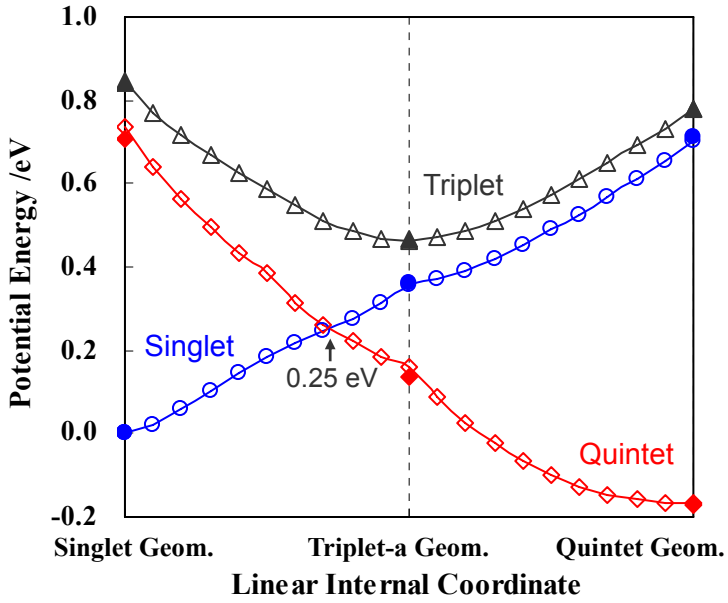

Figure S7. PESs of mer-$[Fe^{II}(2\text{-pic})_3]^{2+}$ in the singlet, triplet, and quintet states, obtained with the B3LYP* method (blanked points, BS-1; filled points, BS-2).

(A) B3LYP

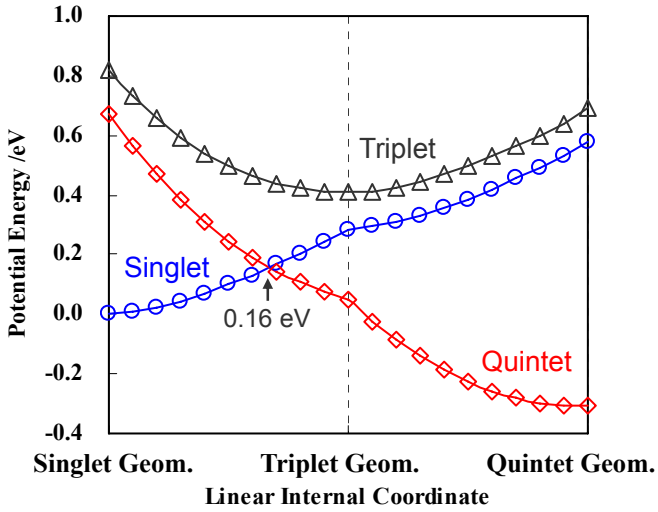

(B) B3LYP*

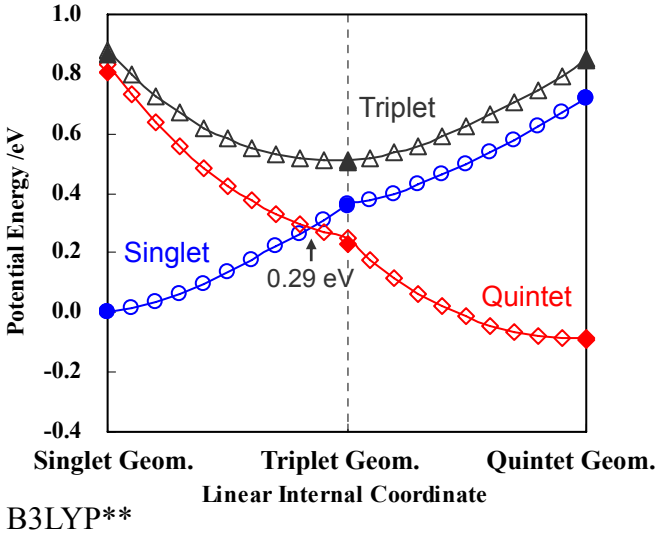

(C) B3LYP**

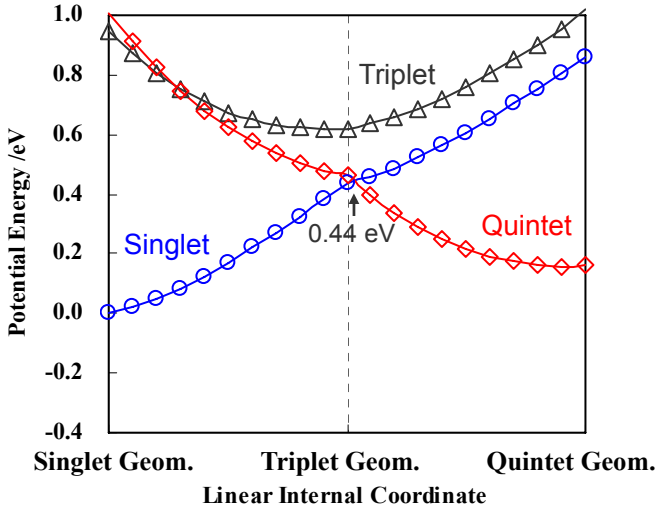

Figure S8. PESs of fac-$[Fe^{II}(2\text{-pic})_3]^{2+}$ in the singlet, triplet, and quintet states. We employed the following three methods; (A) the B3LYP/BS-1 method, (B) the B3LYP* method with BS-1 (blanked points) and BS-2 (filled points), and (C) the B3LYP**/BS-1 method.

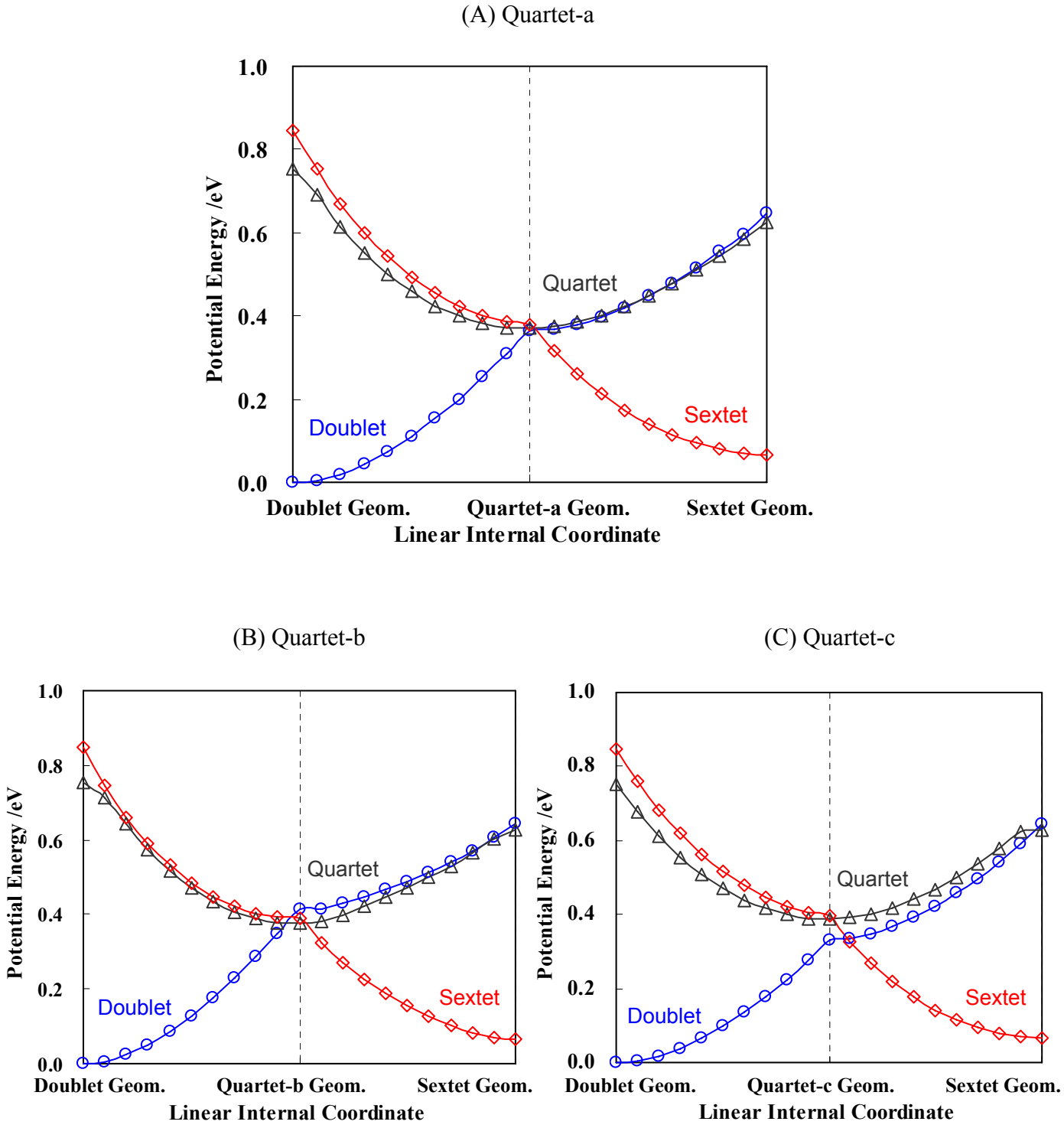

Figure S9. PESs of mer-$[Fe^{III}(2\text{-pic})_3]^{3+}$ in the doublet, quartet, and sextet states (B3LYP/BS-1 calculations). We constructed linear internal coordinates using three Jahn-Teller quartet geometries; (A) the quartet-a, (B) quartet-b, and (C) quartet-c geometries (see Table 2 for these abbreviations).

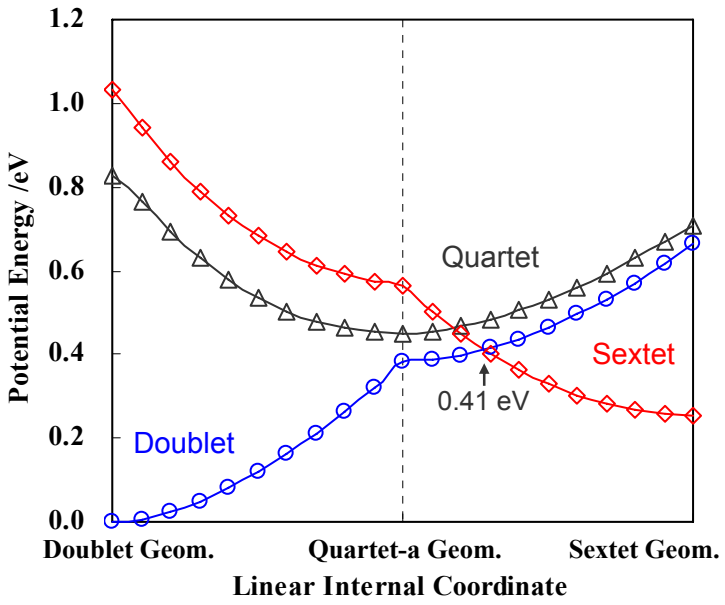

Figure S10. PESs of mer-$[Fe^{III}(2\text{-pic})_3]^{3+}$ in the doublet, quartet, and sextet states, obtained with the B3LYP*/BS-1 method.

(A) B3LYP

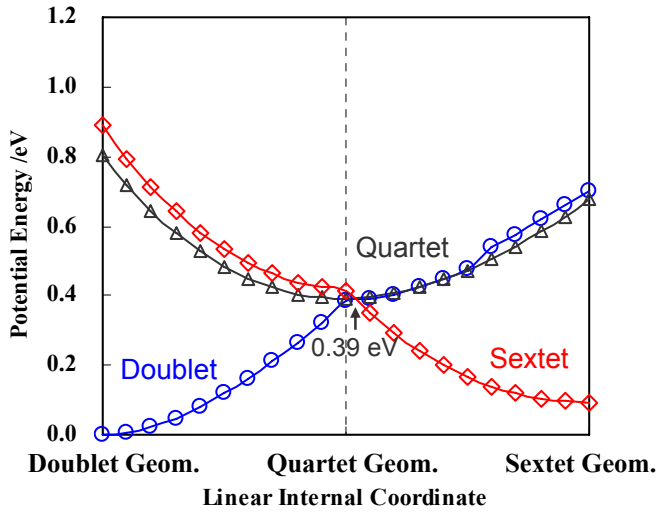

(B) B3LYP*

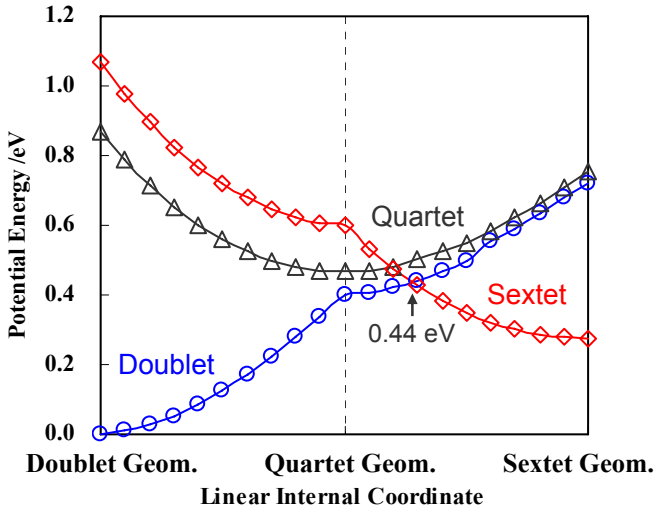

(C) B3LYP**

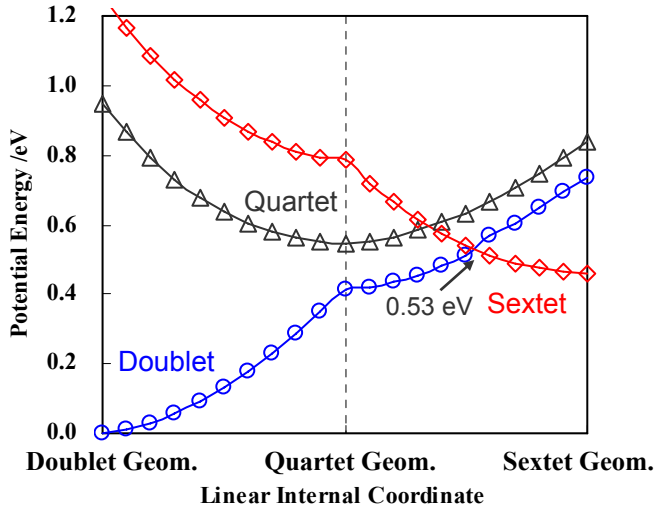

Figure S11. PESs of fac-$[Fe^{III}(2\text{-pic})_3]^{3+}$ in the doublet, quartet, and sextet states. We employed the following three methods; (A) B3LYP method, (B) B3LYP* method, and (C) B3LYP** method with BS-1.

(A) B3LYP

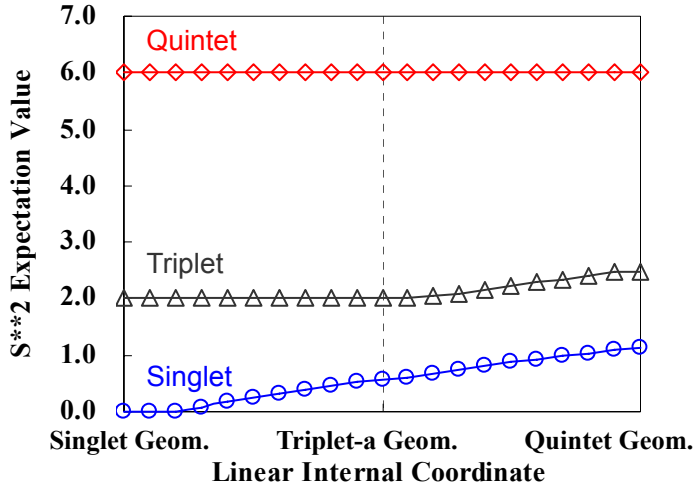

(B) B3LYP*

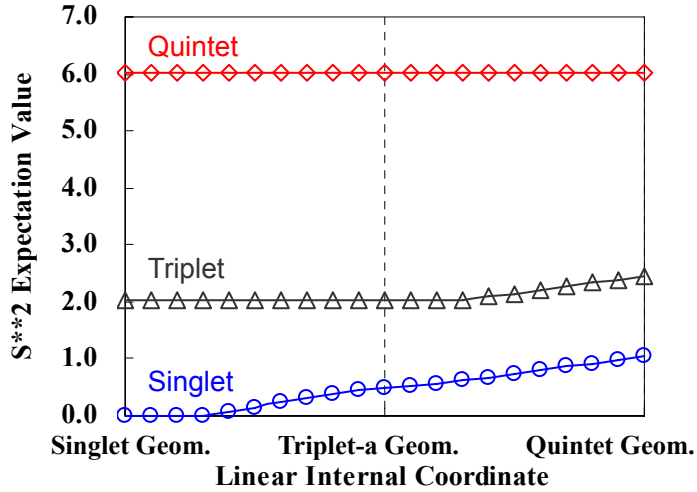

(C) B3LYP**

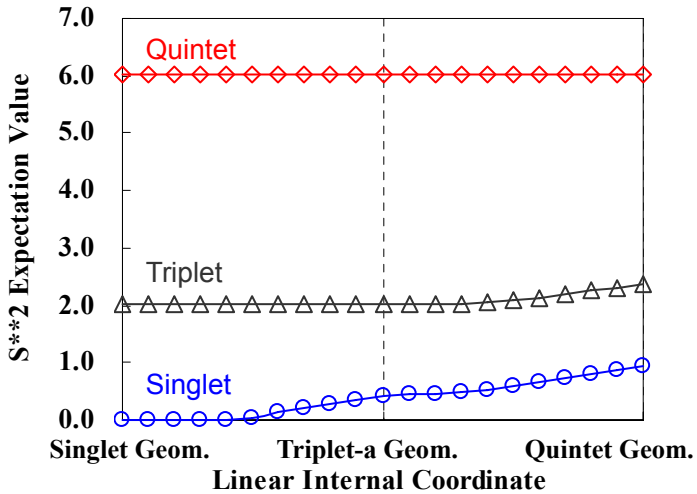

Figure S12. Expectation values of the spin square operator ($\hat{S}^2$) of the singlet, triplet, and quintet wave functions of mer-$[Fe^{II}(2\text{-pic})_3]^{2+}$. The ideal values, or the eigen values, of the singlet, triplet, and quintet states are 0.0, 2.0, and 6.0, respectively. Related potential energy surfaces and linear internal coordinates are shown in Figures 3 and S6A.

Spin contamination problem in the singlet and the triplet states

The spin contamination is very small in the quintet state at all geometries examined here (Figure S12). However, somewhat large spin contamination is observed in the triplet state at the quintet equilibrium geometry. We examined how much the spin contamination influences the potential energy surfaces, as follows: The restricted open-shell B3LYP**-calculated triplet state is more unstable than the restricted B3LYP**-calculated singlet state by 4.2 kcal/mol at the quintet geometry; see Figure S13. Because the singlet state is more stabilized than the triplet state by electron correlation effects, it should be concluded that the singlet state is more stable than the triplet state at the quintet geometry. At the triplet geometry, we could not reach SCF-convergence in the restricted open-shell B3LYP** calculation of the triplet state. However, the spin contamination of the unrestricted B3LYP** calculation is negligibly small in the triplet state (Figure S12), indicating that the total energy of the triplet state at the triplet geometry is correct. The restricted B3LYP**-calculated singlet state is 2.1 kcal/mol more stable than the unrestricted B3LYP**-calculated triplet state at the triplet geometry. Thus, it should be concluded that the singlet state is more stable than the triplet state at the triplet geometry. These results clearly indicate that the discussion based on the unrestricted B3LYP**-calculated PESs (Figure 3) does not change at all by spin contamination.

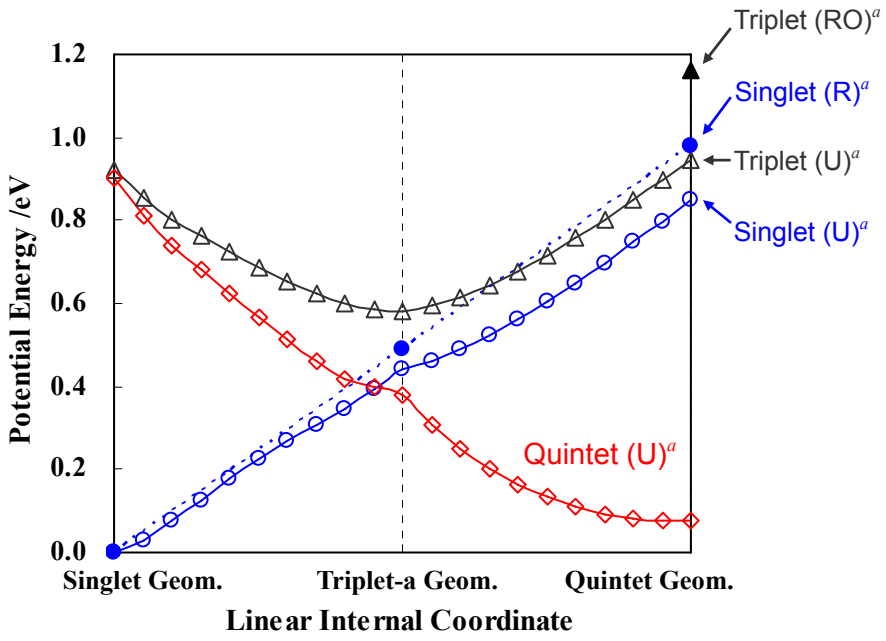

Figure S13. PESs of mer-$[Fe^{II}(2\text{-pic})_3]^{2+}$ in the singlet, triplet, and quintet states, obtained with the B3LYP**/BS-1 method.

[a] RO, R, and U represent the restricted open-shell, restricted closed-shell, and unrestricted open-shell calculations, respectively.

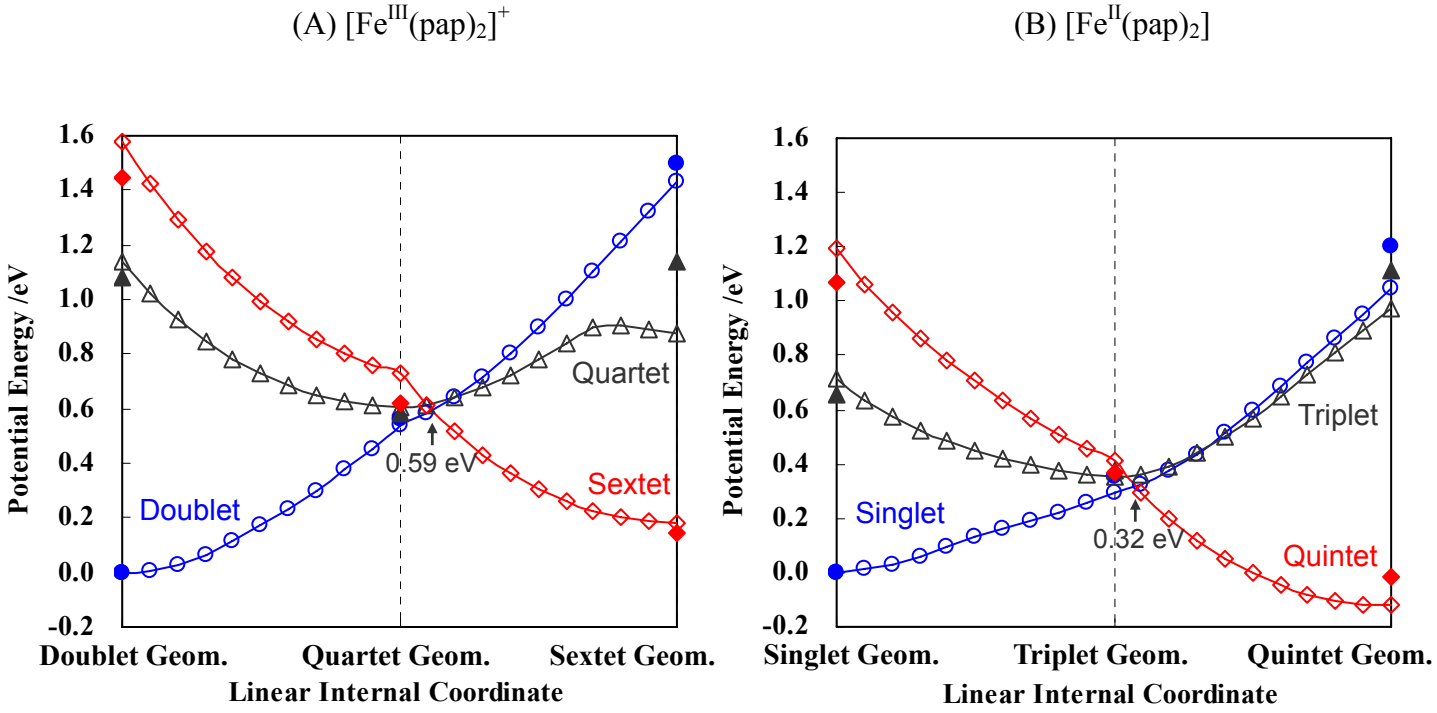

Figure S14. PESs of (A) $[Fe^{III}(pap)_2]^+$ in the doublet, quartet, and sextet states and (B) $[Fe^{II}(pap)_2]$ in the singlet, triplet, and quintet states (blanked points, the B3LYP/BS-3 method; filled points, the B3LYP*/BS-2 method). See footnotes of Tables S7 and S8 for the details of the BS-3 basis set.